NJC

Accepted Manuscript

This is an *Accepted Manuscript*, which has been through the Royal Society of Chemistry peer review process and has been accepted for publication.

Accepted Manuscripts are published online shortly after acceptance, before technical editing, formatting and proof reading. Using this free service, authors can make their results available to the community, in citable form, before we publish the edited article. We will replace this *Accepted Manuscript* with the edited and formatted *Advance Article* as soon as it is available.

You can find more information about *Accepted Manuscripts* in the Information for Authors.

Please note that technical editing may introduce minor changes to the text and/or graphics, which may alter content. The journal's standard Terms & Conditions and the Ethical guidelines still apply. In no event shall the Royal Society of Chemistry be held responsible for any errors or omissions in this *Accepted Manuscript* or any consequences arising from the use of any information it contains.

ROYAL SOCIETY OF CHEMISTRY

www.rsc.org/njc

Journal Name

ARTICLE

Preparation of network-like ZnO/$FeWO_4$ mesoporous heterojunctions with tunable band gaps and their enhanced visible light photocatalytic performance

Received 00th January 20xx,
Accepted 00th January 20xx

DOI: 10.1039/x0xx00000x

www.rsc.org/

Yongchao Ma[a], Yunhua Guo[a], Haiyan Jiang[a], Dan Qu[a], Jing Liu[a], Wukui Kang[a], Ying Yi[a], Wei Zhang[a], Jinsheng Shi[a] and Zhongzhi Han[a]*

Novel mesoporous ZnO/$FeWO_4$ (Zn/$FeWO_4$) heterojunctions with network-like structure were synthesized with a combination of thermal decomposition and hydrothermal method. The samples were characterized by X-ray diffraction (XRD), scanning electron microscopy (SEM), transmission electron microscopy (TEM), X-ray photoelectron spectroscopy (XPS), N_2 sorption and Brunauer-Emmett-Teller (BET) surface area, diffuse reflection spectra (DRS) and photoluminescence spectroscopy (PL). The result showed that the size of $FeWO_4$ was reduced by the modification of ZnO. With the increasing molar ratio of ZnO to $FeWO_4$, the quantum size of $FeWO_4$ decreased from 11 nm to 4 nm, as is followed by a surprisingly band gap broadening. Photocatalytic activity toward degradation of RhB under visible light irradiation was investigated. The optimum decomposition rate of RhB using the prepared 1.5Zn/$FeWO_4$ heterojunction was almost 39 and 9.7 times as that of pristine ZnO and $FeWO_4$, respectively. The active species trapping experiments showed that the holes exhibited an obvious influence on the photocatalytic degradation process. The study on the mechanism showed that the enhanced photocatalytic activity was mainly ascribed to heterojunction construction and band gap broadening, which enhance the efficient transfer and the oxidation potential of holes. This heterojunction shows a potential industrial application to remove undesirable organics from the environment.

1. Introduction

In recent years, semiconductor photocatalysis has attracted considerable interest because it provides a promising pathway for solving environmental pollution and energy shortage 1-4. Metal tungstates belong to an important family of semiconductor with potential application in various fields, such as in catalysis5, photoluminescence6, microwave application7 and humidity sensors8 etc. Among various metal tungstates, monoclinic ferrous tungstate ($FeWO_4$) is a indirect band gap semiconductors with a narrow band gap of 1.8-3.0 eV 9, 10, which matches the solar visible spectrum well. Recently, Yu et al. firstly reported the photocatalytic degradation activity of $FeWO_4$ under modeling sunlight in 2009 11. Kuang et al. reported the photocatalytic decomposition activity of spindle-like $FeWO_4$ nanoparticles under UV irradiation 12. However, the visible light photocatalytic efficiency of $FeWO_4$ is not ideal because of the poor quantum yield caused by the rapid recombination of photogenerated electrons and holes. Thus, it is of considerable significance to develop an efficient strategy to promote the separation efficiency of internal charge carriers of $FeWO_4$ photocatalysts.

As a result, many attempt have been made to overcome these disadvantages, including controlling the morphology10, 11, forming composite structures or heterojunctions13, 14. Construction of a heterostrucutre photocatalyst might be an effective way to enhance the visible light photocatalytic activity of $FeWO_4$, such as $FeWO_4/TiO_2$13, $FeWO_4/Fe_3O_4$14. The enhanced photocatalytic activity of the composites was ascribed to the improvement of charge separation and the interfacial charge transfer efficiency15, 16. It is well known that ZnO has been recognized as an excellent material for photocatalytic process because of its high photosensitivity, low cost and nontoxic nature17, 18. Up to now, some novel photocatalysts have been developed by coupling ZnO with other semiconductors, such as g-C_3N_4/ZnO19, CdS/ZnO heteroarchitecture20, Cu_2O/ZnO21, SnO_2–ZnO heterojunction22, ZnO/BiOI23, and $BiVO_4$–ZnO24, etc. The ZnO-based heterojunction exhibited enhanced photocatalytic activity originating from the efficient separation and transfer of charge carriers. Motivated by these efforts, we intend to design ZnO/$FeWO_4$ heterojunction to enhance the visible light photocatalytic activity of $FeWO_4$. By calculating the energy band positions of ZnO and $FeWO_4$, it was found that the energy levels of $FeWO_4$ and ZnO are well-matched, suiting to construct a heterojunction with efficient electron-hole separation ability. However, to the best of our knowledge, there is

[a] Qingdao Agricultural University, Qingdao 266109, People's Republic of China; E-mail: hanzhongzhiqn@aliyun.com
Tel: +86-532-88030161
Fax: +86-532-86080213

no report on the fabrication of $ZnO/FeWO_4$ heterostructures with efficient photocatalytic activity under visible light irradiation.

Herein, $ZnO/FeWO_4$ mesoporous heterojunctions with network-like structure were, for the first time, prepared by a simple thermal decomposition followed by a hydrothermal process. The modification of ZnO reduced the size of $FeWO_4$, which can significantly tune the band gaps of $ZnO/FeWO_4$ composites. The excellent photocatalytic activity of $ZnO/FeWO_4$ heterojunctions was evaluated by degrading RhB under visible light irradiation. The active species trapping experiments showed that the holes played an important role in the photocatalytic degradation process. In addition, the $ZnO/FeWO_4$ heterojunction also exhibited a high stability and durability after four successive cycles. Finally, the possible photocatalytic mechanism of this heterojunction was proposed based on the investigation of reactive species and the band structure of $FeWO_4$ and ZnO.

2. Experimental

2.1. Materials Synthesis

All the reagents were purchased from Sinopharm Chemical Reagent Co., Ltd. and used directly for experiments without any further purification. Deionized water was used throughout this study. The ZnO sample was synthesized by a facile thermal treatment. Briefly, an appropriate amount of $(ZnCO_3)_2{\cdot}[Zn(OH)_2]_3$ was calcinated at 280 □ in an muffle furnace for 3 h with the heat rate of 10 □ min-1. After being cooled to room temperature, the obtained white products were washed by absolute ethanol and distilled water three times and then dried at 60 □ overnight.

the $ZnO/FeWO_4$ composites were synthesized through a modified solvothermal method 11. Briefly, an appropriate amount of ZnO was dispersed in a mixed solution with 3.5 mL of distilled water and 63 mL of ethylene glycol with ultrasonication for 30 min. Then, 5 mmol of $FeCl_3{\cdot}6H_2O$ was added to the ZnO suspension and stirred magnetically for 30 min. Subsequently, 5 mmol of Na_2WO_4 ·2H2O dissolved in 3.5 mL of distilled water was dropwise added to the above mixture. 10 mmol of sodium acetate was then added to the above mixture with continuous stirring. After 30 min stirring, the above suspension was transferred into a stainless steel autoclave (100 mL) with a Teflon liner and heated at 200 □ for 12 h. After being cooled to room temperature naturally, the obtained products were separated and washed with absolute ethanol and distilled water and then dried at 60 □ for 6 h. The molar ratio of ZnO to FeWO4 in the as-prepared composites was 0.5, 1, 1.5, and 2. And the corresponding samples were denoted as $0.5Zn/FeWO_4$, $1Zn/FeWO_4$, $1.5Zn/FeWO_4$ and $2Zn/FeWO_4$, respectively.

For comparison, the pure $FeWO_4$ sample was prepared with the absence of ZnO under the same conditions. To evaluate the effect of the heterojunction on the photocatalytic activity of the $Zn/FeWO_4$ heterostructures, a mechanically mixed $FeWO_4$ and ZnO sample (M-$1.5Zn/FeWO_4$) was prepared.

2.2 Materials Characterization

The crystalline phases of the $Zn/FeWO_4$ composites were recorded by X-ray diffraction (XRD) with a Bruker D8 diffractometer (Cu Kα radiation, λ=0.15406 nm). The morphology and structure of the as-prepared samples was examined with scanning electron microscope (SEM, S-4800, Hitachi) and transmission electron microscope (TEM, JOEL JEM 2001). X-ray photoelectron spectra (XPS) of the catalysts were recorded in an ESCA-3 Mark II spectrometer (VG Scientific Ltd., England) using Al Kα (1486.6 eV) radiation. Ultraviolet visible (UV-vis) diffuse reflection spectra were measured by means of a UV-vis spectrophotometer (TU-1901, China), which involves an integrating sphere attachment in the range of 200 to 800 nm. $BaSO_4$ was used as the reflectance standard material. The photoluminescence (PL) spectra of the samples were recorded on a Hitachi F-4600 fluorescence spectrophotometer to observe the recombination rate of electron-hole pairs. All of the measurements were performed at room temperature.

2.3 Photocatalytic Test

The photocatalytic activities of the as-prepared products were evaluated by the degradation of RhB dye under visible light irradiation. The photocatalytic reactor (PLS-SXE 300, Beijing Perfect light Co., Ltd.), consists of a quartz glass with a circulating water jack and a 300W Xe lamp with a 420 nm cutoff filter. Typically, an aqueous solution of RhB (100 mL, 10^{-5} M) was placed in a glass, and 30 mg photocatalyst was added. Prior to irradiation, the suspensions were magnetically stirred in the dark for about 60 min to obtain a good adsorption-desorption equilibrium. At 30 min intervals, 5 mL of the solution was taken out and centrifuged to remove the photocatalyst. Then, the filtrates were analyzed by recording variations of the absorption band maximum (553 nm) in the UV-vis spectra of RhB with a TU-1901 spectrophotometer.

2.4. Active species trapping and radical quantification experiments

To detect the active species generated in the photocatalytic process, various scavengers including isopropyl alcohol (IPA,10 mmol L^{-1}), *p*-benzoquinone (*p*-BQ, 1 mmol L^{-1}), and triethanolamine (TEOA, 10 mmol L^{-1}) were introduced into the solution of RhB[25]. The other photocatalytic process was the same as the former photocatalytic activity test (Section 2.3.).

2.5 Photoelectrochemical measurements

The photoelectrochemical characteristics were measured in a CHI660D electrochemical working station using a standard three-compartment cell under Xe arc lamp irradiation with 300 W. In a typical procedure, a commercial ITO glass (1.0 × 1.0 cm^2) was ultrasonicated in an ethanol and distilled water bath prior to use. The clean ITO glass substrate was then immersed in the slurry of the as-prepared photocatalyst (3 mg) and ethanol (3 ml) mixtures. The substrate was then vacuum-dried at 80 °C to eliminate ethanol and subsequently maintained at 100 °C overnight. ITO glass coated with the as-prepared samples, a piece of Pt sheet, a saturated calomel electrode (SCE) and 0.01 M Na_2SO_4 were used as the working electrode, the counter electrode, the reference electrode and the electrolyte, respectively.

3. Results and discussion

The network-like $ZnO/FeWO_4$ mesoporous heterojunction photocatalysts with tunable band gaps have been synthesized via a two-step route. ZnO nanoparticles were first obtained by calcination the corresponding precursors. After that $Zn/FeWO_4$ heterojunctions was prepared with a solvothermal treatment.

3.1. Characterization of samples

Fig. 1 presents the XRD patterns of the as-prepared $FeWO_4$, ZnO, and ZnO modified $FeWO_4$ samples. As shown in Fig. 1a and f, all the diffraction peaks can be well indexed to monoclinic $FeWO_4$ (JCPDS card no.46-1446) and hexagonal ZnO (JCPDS card no. 36-1451), respectively. Besides, no traces of other phases are discovered, indicating the high purity of the samples. For the modified products, the XRD peaks of monoclinic $FeWO_4$ and hexagonal ZnO were observed, confirming the coexistence of ZnO and $FeWO_4$. After modification with ZnO, all the diffraction peaks become broader and weaker, confirming the formation of the nanostructure material[26]. Moreover, the decreased peak intensity of the ZnO modified $FeWO_4$ products indicates the crystal growth inhibition effect between the ZnO and $FeWO_4$[27].

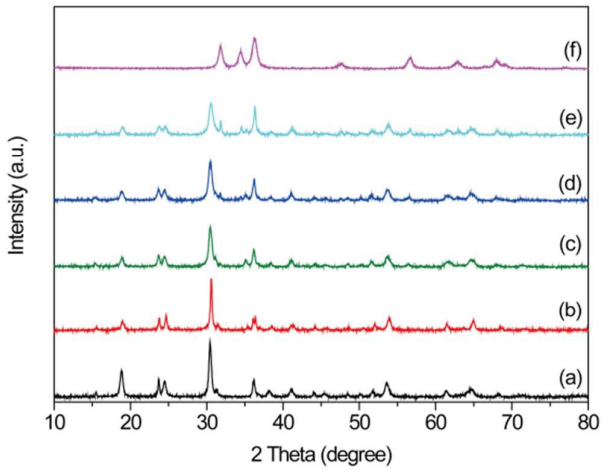

Fig.1. XRD patterns of the as-prepared samples: (a) $FeWO_4$, (b) 0.5Zn/$FeWO_4$, (c) 1Zn/$FeWO_4$, (d) 1.5Zn/$FeWO_4$, (e) 2Zn/$FeWO_4$, and (f) ZnO.

In order to obtain detailed information about the morphology and the nanostructure of the ZnO modified $FeWO_4$ sample, SEM and TEM observations were carried out, and the results are shown in Fig. 2. A typical SEM image (Fig. 2a) shows that the 1.5Zn/$FeWO_4$ composite is composed of numerous nanoparticles with a diameter size in the range of about 10-40 nm. The morphologies of the obtained ZnO, $FeWO_4$, 0.5Zn/$FeWO_4$, 1Zn/$FeWO_4$ and 2Zn/$FeWO_4$ are shown in Fig. S1. Interestingly, compared to the nanoplates of $FeWO_4$, the shapes of Zn/$FeWO_4$ composites are much tiny nanospheres. A low-magnified TEM image of the 1.5Zn/$FeWO_4$ composite shows that the sample has nanosphere morphology with network structure, as presented in Fig. 2b. Furthermore, in order to confirm the relative location of the ZnO and $FeWO_4$ nanoparticles, we made the cross-sectional compositional line profiles of the 1.5Zn/$FeWO_4$ heterojunction (Fig. S2). Fig. S2c shows the EDS analysis result on the place defined by the the small yellow square in Fig. S2a, confirming the existence of Fe, W, Zn and O in this area. Besides, the line profiles of the corresponding compositions (Fig. S2e-f) on the the small yellow square reveal that distribution of Zn in the left location and an increase of Fe in the right location. It is worthwhile to note that each nanoparticles attaches to several other nanoparticles and no self-nucleated and isolated $FeWO_4$ is observed, indicating the formation of Zn/$FeWO_4$ heterojunctions. A typical high-resolution TEM image of the Zn/$FeWO_4$ heterojunctions is shown in Fig. 2c-d. It can be clearly observed that holes with a size of about 3 nm on the surface ZnO nanocrystals and some same pores between nanoparticles (highlighted by circles), indicating the mesoporous nature of Zn/$FeWO_4$ heterojunctions. An interface region was observed in the heterostructures, indicating an intimate contact between the ZnO and $FeWO_4$ nanoparticles (Fig. 2d). The adjacent lattice spacings of the planes are ca. 0.26 and 0.37 nm, corresponding to the (002) planes of hexagonal wurtzite ZnO and (002) planes of monoclinic $FeWO_4$, respectively. There are some nanoparticles on the surface of the ZnO nanocrystals, and the exposed surface of ZnO is easily observed in Fig. 2d.

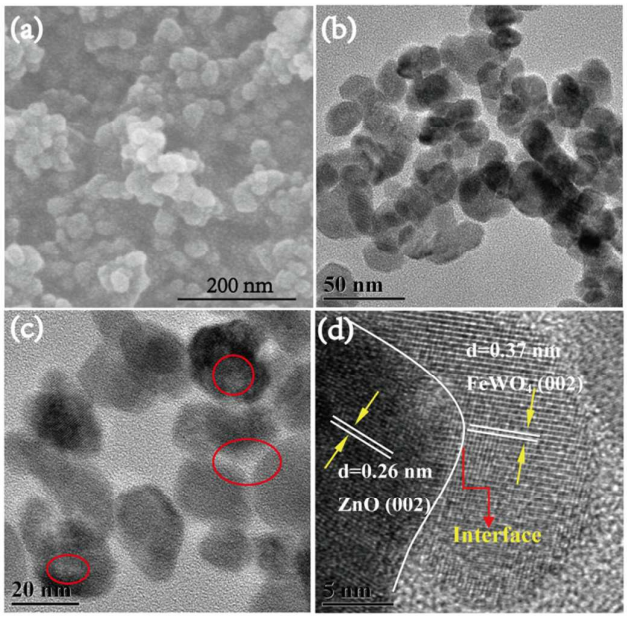

Fig. 2. (a) SEM image, (b) TEM image and (c, d) HRTEM images of the as-synthesized 1.5Zn/$FeWO_4$ heterojunction

Compare to $FeWO_4$ nanoplate, the $FeWO_4$ in the Zn/ $FeWO_4$ composites exhibits a smaller particle size (shown in Fig. S1), which is attributed to the following reasons: (1) in the nucleation process, due to the existence of ZnO, which is employed as a high surface template, the reactants disperse uniformly on its surface. Instead of homogeneous nucleation, the heterogeneous nucleation occurs, which can inhibit the crystal growth. (2) In the process of hydrothermal reaction, the primarily formed crystalline grains distribute uniformly on the surface of ZnO, which can inhibit the further growth of the crystals[28].

The chemical composition and surface chemical states of the as-obtained 1.5Zn/$FeWO_4$ was investigated by XPS, and the corresponding results are shown in Fig. 3. Fig. 3a shows the full spectrum of XPS of the prepared 1.5Zn/$FeWO_4$. The main peaks at 710.9, 35.5, 283.6, 1021.7 and 530.7 eV can be attributed to the binding energies of Fe2p, W4f, C1s, Zn2p and

O1s, respectively. The presence of carbon is mainly from pump oil due to vacuum treatment before the XPS test. In Fig. 3b, the peaks values at 710.4 and 723.9 eV are assigned to the binding energies of Fe $2p_{3/2}$ and Fe $2p_{1/2}$, respectively. In Fig. 3c, two peaks located at 35.5 and 37.8 eV are assigned to W 4f with binding energies corresponding to those of tungsten in the formal valence of +6. From Fig. 3d, it can be observed that the XPS spectrum of Zn 2p shows two individual peaks positioned at 1021.7 and 1044.8 eV, which are assigned to Zn $2p_{3/2}$ and Zn $2p_{1/2}$, respectively[24].

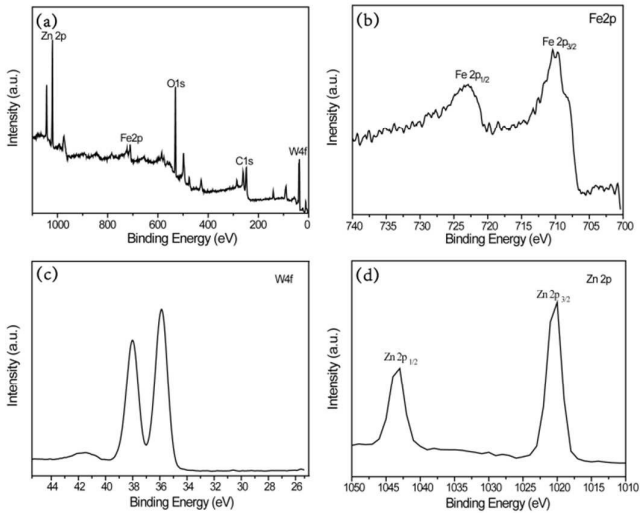

Fig. 3 XPS spectra of the as-obtained 1.5Zn/$FeWO_4$ products: (a) XPS full spectrum, (b) Fe2p, (c) W4f, and (d) Zn2p.

The N_2 adsorption and desorption measurement was used to study the Brunauer-Emmett-Teller (BET) surface areas and porosity of the as-prepared samples. Fig. 4 displays the typical N_2 adsorption/desorption isotherm of $FeWO_4$ and 1.5Zn/$FeWO_4$. As shown in Fig. 4, the N_2 sorption isotherm of $FeWO_4$ and 1.5Zn/$FeWO_4$ is characteristic of type IV with a clear hysteresis loop, suggesting their mesoporous properties[29]. In addition, the insets in Fig. 4 show the pore size distribution of $FeWO_4$ and 1.5Zn/$FeWO_4$. It can be seen that the pore was mainly distributed in the range of 8–40 nm, in agreement to the mesoporous structure. The N_2 adsorption/desorption isotherm of other Zn/$FeWO_4$ composites are shown in Fig. S3. BET surface area (S_{BET}) and the corresponding average pore diameter of the $FeWO_4$ and Zn/$FeWO_4$ products were listed in Table S1. The mesoporous structure is beneficial to the adsorption and transition of RhB or its intermediates during the photocatalytic process.

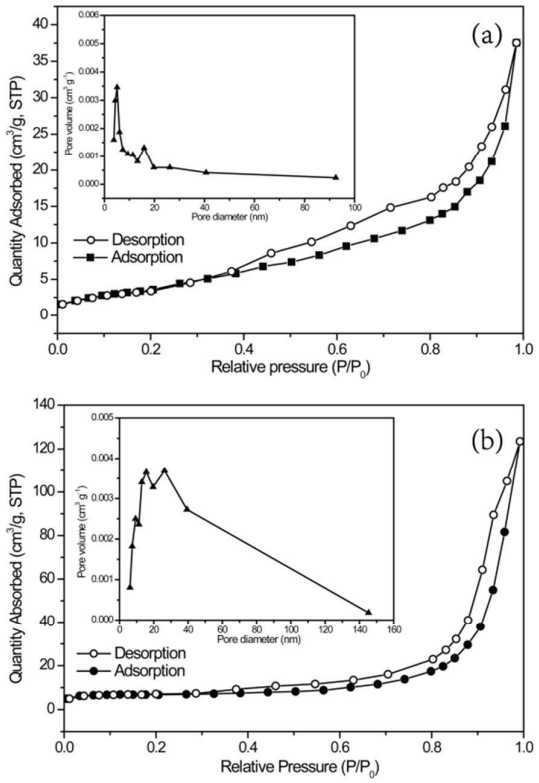

Fig.4. N_2 adsorption-desorption isotherms of (a) $FeWO_4$ sample and (b) 1.5Zn/$FeWO_4$ heterojunction. Inset: pore size distributions of the prepared samples

The optical properties of ZnO, $FeWO_4$, and Zn/$FeWO_4$ heterojunctions were investigated by UV–vis diffuse reflectance spectra, as shown in Fig. 5. The strong absorbance of the white ZnO naoparticles began at around 400 nm, while the brown $FeWO_4$ sample exhibited profound adsorption over the entire visible light region. The fitting directed band gap of ZnO was determined to be 3.2 eV (Fig. S4). It is noted that the Zn/$FeWO_4$ composites showed a broad and strong absorbance from 800 nm to the UV region, indicating the effective photoabsorption of this special structure composition. The indirect band gaps of the $FeWO_4$ and ZnO modified $FeWO_4$ was shown in the Fig. 5 b. With the increasing molar ratio of ZnO, the band gaps of Zn/$FeWO_4$ heterosturcutres show blue shift (Table S2), which are attributed to the quantum confinement of $FeWO_4$ nanoparticles. On the basis of the effective mass approximation model, the blue shift of $FeWO_4$ nanoparticles relative to the bulk is dominated by confinement of electrons and holes, as described by the following equation[30]:

$$\nabla Eg\,(R) = \frac{h^2}{8m_0R^0}\left(\frac{1}{m_e^*} + \frac{1}{m_h^*}\right)$$

where ΔE_g (R) is the band gap shift for the crystal radius R, h the Planck's constant, m_0 the electron mass, while m^*_e and m^*_h are the effective masses of the electrons and holes, respectively. According to the above equation, the calculated sizes of the $FeWO_4$ in the Zn/$FeWO_4$ composites range from 11 to 4 nm (Fig. S5).

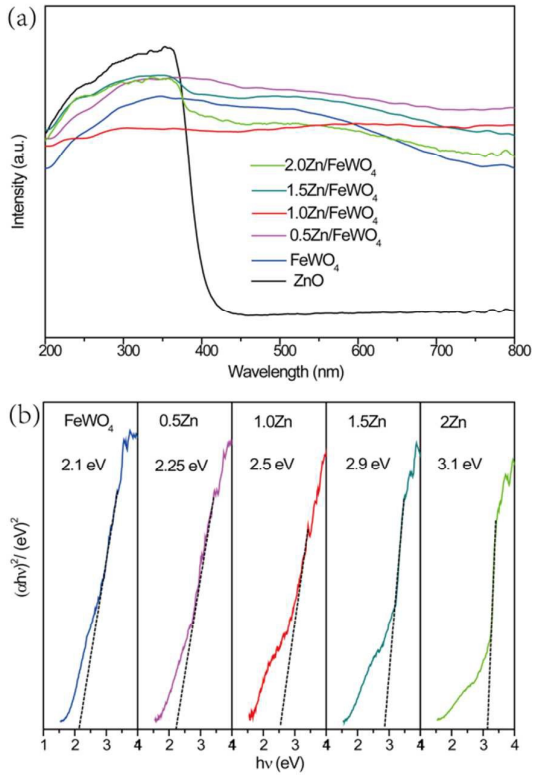

Fig. 5. (a) UV−vis diffuse reflectance spectra of the as-obtained samples. (b) Kubelka-Munk (KM) plot for $FeWO_4$ and $FeWO_4$/ZnO hybrid materials.

The immigration, transfer, and recombination of photogenerated electrons and holes in the Zn/$FeWO_4$ heterostructures were confirmed by PL emission spectra at the room temperature, as shown in Fig. 6. All samples displayed a broad emission band in both the UV and visible region ranging from 330 nm to 600 nm. After the ZnO was introduced, the PL emission intensity of $FeWO_4$ decreased. This may be ascribed to the increase in trap states on the surface defect of Zn/$FeWO_4$ heterostructures[31]. Besides, the visible emission at about 480 nm is the characteristic near-band-edge emission due to the recombination of the free photogenerated electrons and holes[32]. Furthermore, 1.5Zn/$FeWO_4$ and 2Zn/$FeWO_4$ were found to show higher UV emission (indicated by the steep increase in UV region) than the 0.5Zn/$FeWO_4$ and 1Zn/$FeWO_4$. This result indicates the improved crystallinity of ZnO in 1.5Zn/$FeWO_4$ and 2Zn/$FeWO_4$ composites, which is consistent with XRD results[33]. The PL results confirm the importance of the heterojunctions in efficient charge separation.

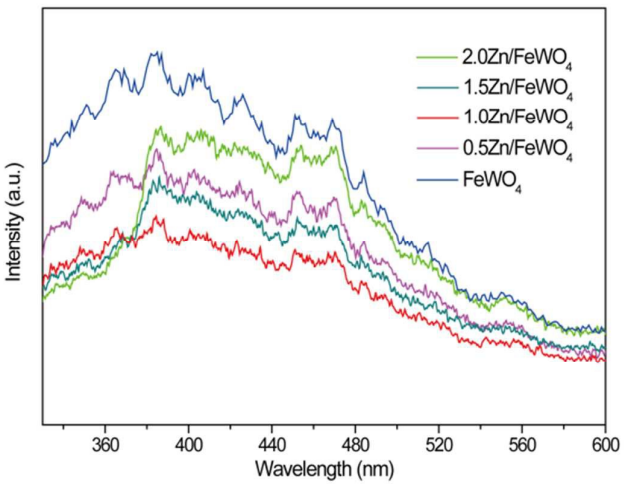

Fig. 6 Photoluminescence (PL) spectra measured at room temperature for $FeWO_4$ and ZnO modified $FeWO_4$ composite photocatalyst. The excitation wavelength was 210 nm.

The effective separation of electron–hole pairs in 1.5Zn/$FeWO_4$ was also confirmed by photocurrent measurement of photocatalyst electrodes (Fig. 7). It can be clearly seen that the rapid and consistent photocurrent responses during on and off cycles of irradiation. It is worth to note that the photocurrent density of the 1.5Zn/$FeWO_4$ heterostructure electrode is higher than that of the pure ZnO and $FeWO_4$ electrode, respectively. The enhanced photocurrent response of the as-prepared mesoporous 1.5Zn/$FeWO_4$ heterostructure indicates higher separation efficiency of the photoinduced electron-hole pairs and a lower recombination rate in such hybrid structures under light illumination. This can be explained by close interfacial connections and the synergetic effect existing in the 1.5Zn/$FeWO_4$ interface.

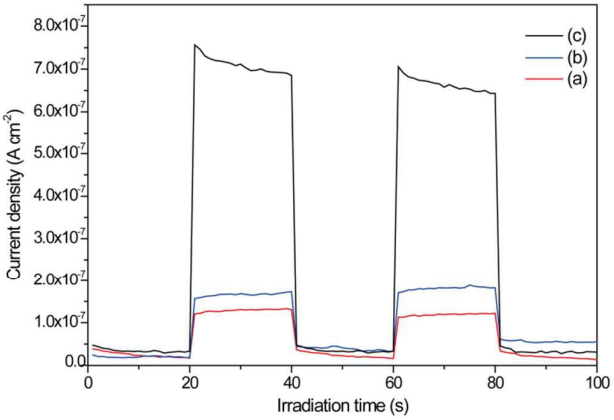

Fig. 7 Photocurrents of the as-prepared samples (a) $FeWO_4$, (b) ZnO, (c) 1.5Zn/$FeWO_4$ with UV-vis light on/off cycles.

3.2 Photocatalytic performance

The photocatalytic activities of ZnO, $FeWO_4$ and Zn/$FeWO_4$ heterojunctions were tested by degradation of RhB solution under visible light irradiation. As shown in Fig. 8a, pure $FeWO_4$ and ZnO could decompose 11% and 23% of RhB solution under irradiation for 150 min. As for the ZnO, The degradation of RhB

might be due to the dye-sensitized process[34]. While, in the case of ZnO modified $FeWO_4$ samples, the 1.5Zn/FWO_4 composite photocatalyst showed better activity than that of single $FeWO_4$ and ZnO. The absorption of RhB over 1.5Zn/FWO_4 significantly decreases with the increase of irradiation time (Fig. S6). The intensity of the adsorption peak at 553 nm nearly disappears after 150 min. It also can be clearly seen that no corresponding increase in absorption is observed in the ultraviolet region, which indicates the complete destruction of most aromatic structures[35]. Besides, the correlation between the $FeWO_4$ quantum sizes and the photocatalytic performances of Zn/$FeWO_4$ was shown in Fig. 8b. It is found that the Zn/$FeWO_4$ with 7 nm $FeWO_4$ nanoparticles exhibits the best photocatalytic performance. However, $FeWO_4$ nanoparticles with larger (7 nm) and smaller (4 nm) sizes make the Zn/$FeWO_4$ with inferior photocatalytic performance.

The degradation kinetics of RhB under visible light irradiation over the as-obtained samples was investigated by the Langmuir-Hinshelwood model[27], as shown in Fig. S7. The apparent rate constants for the prepared photocatalysts were summary in Table S2. Especially, the decomposition of RhB over the 1.5 Zn/FWO_4 heterojunction (0.0058 min^{-1}) is faster than that of $FeWO_4$ (0.0002 min^{-1}) and ZnO (0.0006 min^{-1}) by a factor of 29 and 9.7, respectively. To further confirm the heterojunction effect on the present system, the photocatalytic experiment of the M-1.5Zn/$FeWO_4$ sample is also investigated. The photocatalytic activity of the M-1.5Zn/$FeWO_4$ samples is much lower than that of the 1.5Zn/$FeWO_4$ (Fig. S8). This result demonstrates that the 1.5Zn/$FeWO_4$ composite can form intimate interfaces in the heterojunction, rather than form loose interfaces in the mechanically mixed samples [15, 36].

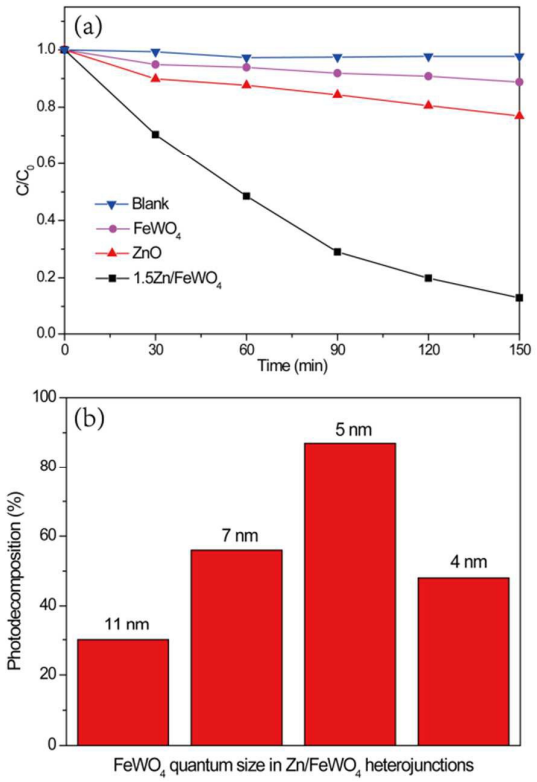

Fig. 8 (a) Photocatalytic decomposition of RhB solution over different samples under visible light irradiation, and (b) the effect of FeWO4 size on the photocatalytic efficiencies of the ZnO modified FeWO4 heterojunctions.

In addition to photocatalytic efficiency, the stability of photocatalysts was another important factor for practical application[37]. The 1.5Zn/$FeWO_4$ heterojunction was recycled in four successive photocatalytic experiments. As shown in Fig. 9a, the photocatalytic activity of 1.5Zn/$FeWO_4$ sample exhibits no significant loss after four recycles for the photodegradation of RhB solution. Fig. 9b presents the XRD patterns of 1.5Zn/$FeWO_4$ before and after four runs under visible light for the degradation of RhB solution. It can be clearly observed that the heterojunction is stable during the photocatalytic degradation process.

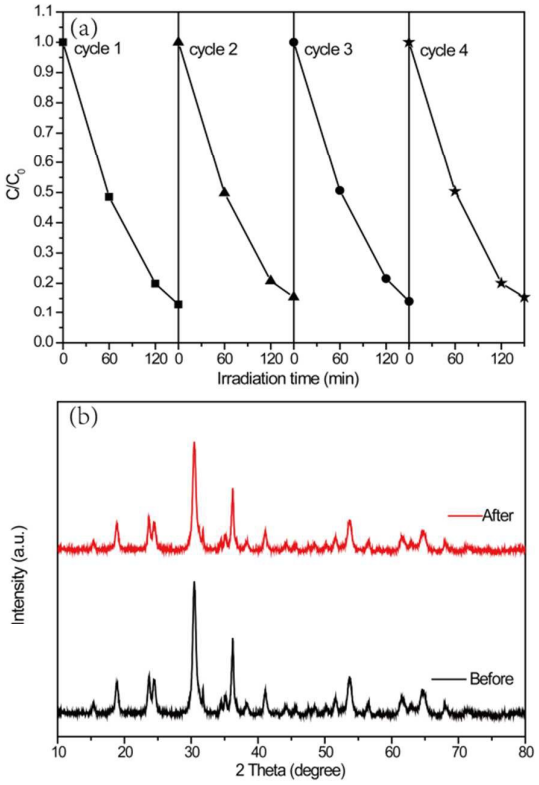

Fig. 9 (a) Recycling tests of 1.5Zn/$FeWO_4$ under visible light irradiation, (b) XRD patterns of the 1.5Zn/$FeWO_4$ before and after photocatalytic degradation of RhB solution with four cycles.

3.3 Photocatalytic mechanism

The activity of photocatalysts is mostly governed by surface area, adsorption ability and separation efficiency of photogenerated carriers[38]. The comparison of the adsorption ability and reaction kinetics of photocatalytic degradation of RhB dye in the presence of different products was shown in Fig. 10. Without visible irradiation, the adsorption ability of composite samples follows the trend: 1.5Zn/$FeWO_4$> 0.5Zn/$FeWO_4$> 2Zn/$FeWO_4$> 1Zn/$FeWO_4$. However, the degradation rate does not follow the dye adsorption trend. The 1.5Zn/$FeWO_4$ heterojunction obviously showed higher photocatalytic activity under identical experimental conditions, followed by 2Zn/$FeWO_4$, and then 1Zn/$FeWO_4$, and 0.5Zn/$FeWO_4$. As a catalyst, the surface area is an important factor for its catalytic activity[39, 40]. However, the N_2 adsorption-desorption measurements confirmed that the order of the photocatalytic performance of various photocatalysts is not consistent with the order of the surface area. That is to say, the enhanced photocatalytic activity is not due to the surface area but for other reasons. In this system, the enhancement of photocatalytic activity of Zn/$FeWO_4$ heterojunction was mainly ascribed to efficient charge separation of photogenerated carriers.

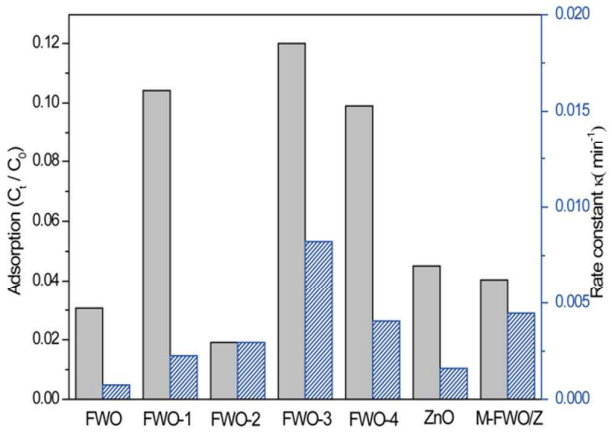

Fig. 10 Comparison of reaction rate constant and adsorption ability of various photocatalysts: (a) $FeWO_4$, (b) 0.5Zn/$FeWO_4$, (c) 1Zn/$FeWO_4$, (d) 1.5Zn/$FeWO_4$, (e) 2Zn/$FeWO_4$, (f), (g) M-1.5Zn/$FeWO_4$.

The active species in the photocatalytic reactions of RhB were investigated by adding different scavengers, and the results are shown in Fig. 11. When the triethanolamine (TEOA, a holes radical scavenger) is added into the reaction system, the degradation efficient of RhB is obviously inhibited. When the benzoquinone (BQ) scavenger for superoxide radicals ($O_2^{\cdot-}$) are added into the reaction system, no obvious effect on the photocatalytic activity of 1.5Zn/$FeWO_4$was observed. Moreover, once the isopropyl alcohol (IPA) scavenger for hydroxyl radicals is added to the reaction system, a slight inhibition phenomenon for photocatalytic reaction is observed. These results clearly suggest that the photocatalytic oxidation of RhB of 1.5Zn/$FeWO_4$ heterojunction is mainly driven by photo-generated holes[35]. The $O_2^{\cdot-}$ plays the less important role than those of holes and hydroxyl radicals in photocatalytic oxidation of RhB dye.

Fig. 11 Effects of different active scavengers on the degradation RhB over 1.5Zn/$FeWO_4$ composite.

The energy band positions of $FeWO_4$ and ZnO were estimated according to the following empirical equations [41]:

$$E_{CB} = X - E^C - \frac{1}{2}E_g \quad (2)$$

$$E_{VB} = E_{CB} + E_g \quad (3)$$

Where E_{VB} and E_{CB} is the valence band (VB) and conduction band (CB) edge potentials, respectively; X represents the absolute electronegativity of the semiconductor, which is defined as the geometric mean for absolute electronegativity of the constituent atoms. E^C is the energy of free electrons on the hydrogen scale (about 4.5 eV), and E_g is the band gap energy of the semiconductor[42]. The energy band parameters of $FeWO_4$ and ZnO were calculated, and listed in Table S3. Band position calculations suggest ZnO and $FeWO_4$ have the staggered energy potentials that can reduce the combination of the photogenerated carriers between the two semiconductors.

Based on the above analysis results, we proposed the possible mechanism of enhanced photocatalytic activity of the Zn/$FeWO_4$ heterojunction. Schematic diagram of band energy positions and the charge transfer process of the Zn/$FeWO_4$ heterojunction under visible light irradiation were shown in Fig. 12. The position of CB bottom and the VB top of $FeWO_4$ (0.76 eV and 2.86 eV, respectively) are lower than those of ZnO (-0.40 eV and 2.80 eV, respectively). Besides, $FeWO_4$ could be simultaneously excited to form electron-hole pairs under visible light irradiation. Consequently, the photogenerated holes could easily transfer from the CB of the $FeWO_4$ to that of ZnO, and further react with H_2O adsorbed on the surface of the heterojunction to produce·OH. Then the resulting·OH and a certain amount of h^+ could decompose the RhB dye to the final products. However, to continue the catalytic reaction, the electrons in the VB of $FeWO_4$ must be scavenged. Given the fact that the CB level of $FeWO_4$ (+0.76 eV vs. NHE) is more positive than $E_0(O_2/O_2^{\cdot-})$=-0.046 eV vs NHE), adsorbed O_2 cannot be directly transferred to oxygen species by electrons in CB of $FeWO_4$. Hence, the electrons in the $FeWO_4$ CB are transported to the oxygen species through the multi-electron process [43]. Therefore, the electron-hole pairs were separated efficiently on the Zn/$FeWO_4$ heterojunction interface. On the other hand, as the sizes of $FeWO_4$ nanoparticles decrease, the band gaps of Zn/$FeWO_4$ become lager because of the quantum confinement of $FeWO_4$. However, the valence band of $FeWO_4$ shifts to more positive potentials to result in the larger valence band energy difference between $FeWO_4$ and ZnO, which enhances the efficient transfer and the oxidation potential of holes.

Furthermore, in the process of RhB photosensitization, the electrons on the electrons on the highest occupied molecular orbital (HOMO) of RhB molecules will be excited to the lowest unoccupied molecular orbital (LUMO) under visible light, and subsequently would be injected to the CB bottom of ZnO, further taking part in the degradation of RhB.

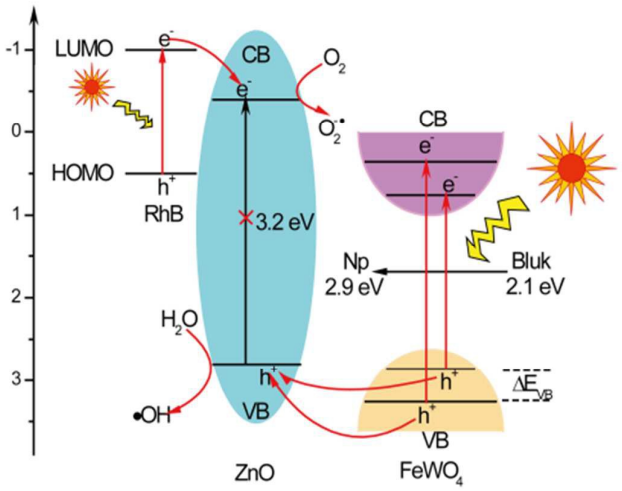

Fig. 12 Schematic diagram of band energy positions and the charge transfer process of the Zn/$FeWO_4$ heterojunction under visible light irradiation.

4. Conclusions

In summary, the mesoporous Zn/$FeWO_4$ heterojunctions with tunable band gaps have been successfully synthesized by a simple two-step method. ZnO nanoparticles were first prepared by calcination treatment of the precursors. And subsequently Zn/$FeWO_4$ heterojunctions were formed with a solvothermal process. SEM and TEM confirmed that the size of $FeWO_4$ was reduced by the modification of ZnO. Thus, the band gaps of $FeWO_4$ were significantly tuned, which can be demonstrated by the DRS analysis. The photocatalytic performance of Zn/$FeWO_4$ heterojunctions was better than that of pure $FeWO_4$ and ZnO. The optimal molar ratio of ZnO to $FeWO_4$ was 1.5 with the maximal photocatalytic degradation efficiency of 87% under the visible light irradiation for 3 h. The active species trapping experiments showed that the holes exhibited an obvious influence on the photocatalytic degradation process. Our preliminary experimental results showed that the remarkable enhancement of photocatalytic performance is mainly due to the efficient transfer and tunable band gaps. Moreover, this novel Zn/$FeWO_4$ heterojunction could be easily recycled several times, which is expected to show considerable potential application in wastewater treatment.

Acknowledgements

This work is financially supported by Science and Technology Development Plan of Shandong Province, China (2014GNC110013) and Graduate Innovation Fund of Qingdao Agricultural University (QYC201422).

Notes and references

1. L. Zhang, S. Li, B. Liu, D. Wang and T. Xie, *ACS Catalysis*, 2014, 4, 12319.

2. H. Lin, L. Li, M. Zhao, X. Huang, X. Chen, G. Li and R. Yu, *Journal of the American Chemical Society*, 2012, 134, 8328.
3. P. Gao, A. Li, D. D. Sun and W. J. Ng, *J Hazard Mater*, 2014, 279, 96.
4. S. Li, J. Cai, X. Wu, F. Zheng, X. Lin, W. Liang, J. Chen, J. Zheng, Z. Lai, T. Chen and L. Zhu, *Applied Catalysis B: Environmental*, 2014, 160–161, 279.
5. Y. Wang, X. Guan, L. Li, H. Lin, X. Wang and G. Li, *New J Chem*, 2012, 36, 1852.
6. Y. Chen, S. W. Park, B. K. Moon, B. C. Choi, J. H. Jeong and C. Guo, *CrystEngComm*, 2013, 15, 8255.
7. J. Zhang, Y. Zhang, J.-Y. Yan, S.-K. Li, H.-S. Wang, F.-Z. Huang, Y.-H. Shen and A.-J. Xie, *Journal of Nanoparticle Research*, 2012, 14, 1.
8. Y.-X. Zhou, Q. Zhang, J.-Y. Gong and S.-H. Yu, *The Journal of Physical Chemistry C*, 2008, 112, 13383.
9. J. Zhang, Y. Wang, S. Li, X. Wang, F. Huang, A. Xie and Y. Shen, *CrystEngComm*, 2011, 13, 5744-5750.
10. F. Yu, L. Cao, J. Huang and J. Wu, *Ceramics International*, 2013, 39, 4133.
11. Y.-X. Zhou, H.-B. Yao, Q. Zhang, J.-Y. Gong, S.-J. Liu and S.-H. Yu, *Inorg Chem*, 2009, 48, 1082.
12. J. Guo, X. Zhou, Y. Lu, X. Zhang, S. Kuang and W. Hou, *J Solid State Chem*, 2012, 196, 550.
13. S. Bera, S. B. Rawal, H. J. Kim and W. I. Lee, *ACS applied materials & interfaces*, 2014, 6, 9654.
14. X. Cao, Y. Chen, S. Jiao, Z. Fang, M. Xu, X. Liu, L. Li, G. Pang and S. Feng, *Nanoscale*, 2014, 6, 12366.
15. Y. Tian, B. Chang, J. Lu, J. Fu, F. Xi and X. Dong, *ACS applied materials & interfaces*, 2013, 5, 7079.
16. A. Iwase, Y. H. Ng, Y. Ishiguro, A. Kudo and R. Amal, *Journal of the American Chemical Society*, 2011, 133, 11054.
17. Z. Wang, S.-W. Cao, S. C. J. Loo and C. Xue, *CrystEngComm*, 2013, 15, 5688.
18. A. McLaren, T. Valdes-Solis, G. Li and S. C. Tsang, *Journal of the American Chemical Society*, 2009, 131, 12540.
19. Y. Wang, R. Shi, J. Lin and Y. Zhu, *Energ Environ Sci*, 2011, 4, 2922.
20. S. Liu, M.-Q. Yang, Z.-R. Tang and Y.-J. Xu, *Nanoscale*, 2014, 6, 7193.
21. X. Zou, H. Fan, Y. Tian and S. Yan, *CrystEngComm*, 2014, 16, 1149.
22. L. Zheng, Y. Zheng, C. Chen, Y. Zhan, X. Lin, Q. Zheng, K. Wei and J. Zhu, *Inorg Chem*, 2009, 48, 1819.
23. J. Jiang, X. Zhang, P. Sun and L. Zhang, *The Journal of Physical Chemistry C*, 2011, 115, 20555.
24. S. Balachandran, N. Prakash, K. Thirumalai, M. Muruganandham, M. Sillanpää and M. Swaminathan, *Ind Eng Chem Res*, 2014, 53, 8346.
25. Y. Bai, P.-Q. Wang, J.-Y. Liu and X.-J. Liu, *RSC Advances*, 2014, 4, 19456.
26. S. Martha, K. H. Reddy and K. M. Parida, *Journal of Materials Chemistry A*, 2014, 2, 3621.
27. K. H. Reddy, S. Martha and K. M. Parida, *Inorg Chem*, 2013, 52, 6390.
28. W. Wang, L. Hu, J. Ge, Z. Hu, H. Sun, H. Sun, H. Zhang, H. Zhu and S. Jiao, *Chemistry of Materials*, 2014, 26, 3721.
29. J. Xu, M. Chen and Z. Wang, *Dalton Transactions*, 2014, 43, 3537.
30. H. Cheng, B. Huang, X. Qin, X. Zhang and Y. Dai, *Chem Commun*, 2011, 48, 97.
31. W. Zhao, Y. Wang, Y. Yang, J. Tang and Y. Yang, *Applied Catalysis B: Environmental*, 2012, 115, 90.
32. Z. Wu, L. Chen, C. Xing, D. Jiang, J. Xie and M. Chen, *Dalton Transactions*, 2013, 42, 12980-12988.
33. F. Liu, Y. H. Leung, A. B. Djurišić, A. M. C. Ng and W. K. Chan, *The Journal of Physical Chemistry C*, 2013, 117, 12218.
34. J. Cao, B. Xu, H. Lin, B. Luo and S. Chen, *Dalton Transactions*, 2012, 41, 11482.
35. H. Li, J. Liu, W. Hou, N. Du, R. Zhang and X. Tao, *Applied Catalysis B: Environmental*, 2014, 160–161, 89.
36. C. Chang, L. Zhu, S. Wang, X. Chu and L. Yue, *ACS applied materials & interfaces*, 2014, 6, 5083.
37. Y. Yang, W. Guo, Y. Guo, Y. Zhao, X. Yuan and Y. Guo, *J Hazard Mater*, 2014, 271, 150.
38. L.-W. Zhang, H.-B. Fu and Y.-F. Zhu, *Advanced Functional Materials*, 2008, 18, 2180.
39. F. Amano, K. Nogami, M. Tanaka and B. Ohtani, *Langmuir*, 2010, 26, 7174.
40. N. M. Flores, U. Pal, R. Galeazzi and A. Sandoval, *RSC Advances*, 2014, 4, 41099.
41. H.-q. Jiang, H. Endo, H. Natori, M. Nagai and K. Kobayashi, *Materials Research Bulletin*, 2009, 44, 700.
42. D.-K. Ma, M.-L. Guan, S.-S. Liu, Y.-Q. Zhang, C.-W. Zhang, Y.-X. He and S.-M. Huang, *Dalton Trans.*, 2012, 41, 5581.
43. L. Ye, J. Liu, Z. Jiang, T. Peng and L. Zan, *Applied Catalysis B: Environmental*, 2013, 142–143, 1.

Graphical Abstract

The enhanced photocatalytic activity of ZnO/$FeWO_4$ composite is ascribed to both construct heterojunction and its tunable band gaps.